UCLA/00/TEP/33
CWRU-P13-00
December 2000

WIMP Annual Modulation with Opposite Phase in Late-Infall Halo Models

Graciela Gelmini[1], Paolo Gondolo[2]

[1] *Dept. of Physics and Astronomy, UCLA (University of California, Los Angeles)*
405 Hilgard Ave., Los Angeles CA 90095, USA
gelmini@physics.ucla.edu

[2] *Dept. of Physics, Case Western Reserve University*
10900 Euclid Ave., Cleveland, OH 44106-7079, USA
pxg26@po.cwru.edu

Abstract

We show that in the late-infall model of our galactic halo by P. Sikivie the expected phase of the annual modulation of a WIMP halo signal in direct detection experiments is opposite to the one usually expected. If a non-virialized halo component due to the infall of (collisionless) dark matter particles cannot be rejected, an annual modulation in a dark matter signal should be looked for by experimenters without fixing the phase a-priori. Moreover, WIMP streams coming to Earth from directions above and below the galactic plane should be expected, with a characteristic pattern of arrival directions.

1 Introduction

The dark halo of our galaxy may consist of WIMPs (weakly interacting massive particles). Direct detection experiments attempt to measure the nuclear recoil caused by these dark matter particles interacting with the material in a detector. The most important signature of a halo dark matter signal in these experiments is its annual modulation [1]. The WIMP interaction rate, the energy deposited

per collision, as well as the annual modulation of the signal depend strongly on the velocity distribution of the halo dark matter particles with respect to the detector. It is therefore very important to explore the possibility of halo particles velocity distributions which differ from the one usually assumed. The standard assumption is of a virialized dark halo, on average at rest in the rest frame of the galaxy, with a gaussian velocity distribution truncated due to the escape velocity from the galaxy, of about 600 km/s. The average WIMP velocity on Earth in then due to the motion of the Earth with respect to the galaxy (at about 200 km/s). This velocity is maximal around June 2 each year, when the velocity of the Earth around the Sun adds up maximally to the velocity of the Sun with respect to the galaxy, and minimal six months later, around December 2 each year.

A non-standard halo model is the late-infall model of Refs. [3], modified in recent years by P. Sikivie and collaborators [4, 5, 6]. It assumes a non-virialized dark halo in which collisionless dark matter particles falling into the galaxy oscillate in and out many times. At a given location in the galaxy, multiple flows of particles are possible, each having a specific velocity in a specific direction. The non-virialized flows of dark matter particles produce a velocity distribution completely different from the standard truncated Gaussian. The particular late-infall model of Sikivie in Ref. [6] is a self-similar axially symmetric infall model with net angular momentum and parameters adjusted to describe well our galaxy. For this model, which we call Sikivie's LI model or SLI model from now on, the local velocities and densities of the first twenty pairs of flows are given in Table 1 of Ref. [6]. We reproduce this table in our Table 1 for convenience. The first pair of flows corresponds to particles coming into the galaxy for the first time from opposite sides of it, the second to those passing for the second time, etc.

Here we would like to clearly expose the differences that this particular late infall halo model by Sikivie implies for direct dark matter detection experiments.

2 Characteristics of the WIMP Wind

In the first comparison between the standard halo model and Sikivie's late infall model, we consider the flux of WIMPs as a function of solid angle for an observer moving with the Sun. If $\mathbf{v}$ is the velocity of a WIMP with respect to the galaxy, its velocity $\mathbf{u}$ with respect to the Sun is simply given by a galilean transformation

$$\mathbf{u} = \mathbf{v} - \mathbf{v}_\odot, \tag{1}$$

where

$$\mathbf{v}_\odot = \mathbf{v}_{\rm LSR} + \mathbf{v}'_\odot. \tag{2}$$

$\mathbf{v}_\odot$ is the velocity of the Sun with respect to the galactic rest frame, $\mathbf{v}_{\rm LSR}$ is the velocity of the Local Standard of Rest (LSR), which is in the direction of galactic rotation, and $\mathbf{v}'_\odot$ is the peculiar velocity of the Sun, i.e. its velocity with respect to the LSR. In a coordinate system in which X points toward the

i	ρ_i (10^{-26} g/cm^3)	v_{iX} (km/s)	v_{iY} (km/s)	v_{iZ} (km/s)	u_i^+, u_i^- (km/s)
$1^\pm$	0.4	0	140	$\pm$605	605, 619
$2^\pm$	1.0	0	255	$\pm$505	499, 513
$3^\pm$	2.0	0	350	$\pm$390	401, 414
$4^\pm$	6.3	0	440	$\pm$240	312, 322
$5^\pm$	9.2	$\pm$190	440	0	274, 288
$6^\pm$	2.9	$\pm$295	355	0	310, 329
$7^\pm$	1.9	$\pm$330	290	0	325, 345
$8^\pm$	1.4	$\pm$350	250	0	340, 360
$9^\pm$	1.1	$\pm$355	215	0	346, 365
$10^\pm$	1.0	$\pm$355	190	0	348, 368
$11^\pm$	0.9	$\pm$355	170	0	351, 370
$12^\pm$	0.8	$\pm$350	150	0	350, 369
$13^\pm$	0.7	$\pm$345	135	0	349, 368
$14^\pm$	0.6	$\pm$340	120	0	349, 368
$15^\pm$	0.6	$\pm$330	110	0	343, 362
$16^\pm$	0.55	$\pm$325	100	0	342, 360
$17^\pm$	0.50	$\pm$320	90	0	341, 360
$18^\pm$	0.50	$\pm$310	85	0	335, 353
$19^\pm$	0.45	$\pm$305	80	0	333, 350
$20^\pm$	0.45	$\pm$300	75	0	330, 348

Table 1: Local densities and velocities of the first 20 pairs of flows in the self-similar infall model of ref. [5]. The first five columns are from Table 1 in Ref. [6]. The last column gives the flow speeds with respect to the Sun (as obtained by us).

galactic center, Y toward the direction of galactic rotation, and Z toward the North Galactic Pole, we adopt

$$\mathbf{v}_{\rm LSR} = (0, 220, 0)\,{\rm km/s}, \tag{3}$$

for the velocity of the Local Standard of Rest, and

$$\mathbf{v}_\odot = (10, 13, 7)\,{\rm km/s} \tag{4}$$

for the Sun peculiar velocity. (The uncertainty in the Sun peculiar velocity is of the order of 0.2 km/s in the Z direction and of as much as 3 km/s in the X and Y directions [2]; the corresponding uncertainty in the phase constant of the modulation we discuss below is of several days.)

With these preliminaries, the flux of WIMPs arriving at the Sun from within the solid angle $d\Omega$ around the direction $\hat{\mathbf{n}}$ is

$$\frac{d\Phi}{d\Omega} = \frac{\rho}{m}\int u f_\odot(-u\hat{\mathbf{n}})\cdot u^2 du. \tag{5}$$

Here ρ is the local halo density, m is the WIMP mass, and $f_\odot(\mathbf{u})d^3u$ is the fraction of WIMPs with velocities with respect to the Sun within d^3u around $\mathbf{u}$. The WIMP velocity distribution in the rest frame of the Sun $f_\odot(\mathbf{u})$ is related to the WIMP velocity distribution in the galactic rest frame $f(\mathbf{v})$ through

$$f_\odot(\mathbf{u}) = f(\mathbf{u}+\mathbf{v}_\odot). \tag{6}$$

Below we plot the WIMP flux $d\Phi/d\Omega$ as a function of the arrival direction $\hat{\mathbf{n}}$ in galactic coordinates (l, b), $\hat{\mathbf{n}} = (\cos b\cos l, \cos b\sin l, \sin b)$. We do this for two models of the velocity distribution: the standard halo model and the late-infall model of Sikivie and collaborators.

In the standard halo model, the WIMP velocity distribution is assumed to be a gaussian with velocity dispersion $\overline{v}_0/\sqrt{2}$ truncated at the escape velocity $v_{\rm esc}$,

$$f_{\rm std}(\mathbf{v}) = \begin{cases} \dfrac{1}{N_{\rm esc}\pi^{3/2}\overline{v}_0^3}\, e^{-\mathbf{v}^2/\overline{v}_0^2}, & \text{for } |\mathbf{v}| < v_{\rm esc} \\ 0, & \text{otherwise,} \end{cases} \tag{7}$$

where ρ is the local WIMP density, m is the WIMP mass, and $N_{\rm esc} = {\rm erf}(z_0) - 2z_0\exp(-z_0^2)/\pi^{1/2}$ with $z_0 = v_{\rm esc}/\overline{v}_0$ is a normalization factor. For the sake of illustration, we take $\overline{v}_0 = 220$ km/s and $v_{\rm esc} = 650$ km/s. Other values do not change our conclusions.

A simple integration gives the flux per unit solid angle as

$$\frac{d\Phi_{\rm std}}{d\Omega} = \frac{\rho v_\odot}{m}\, h_0(l, b), \tag{8}$$

where $v_\odot = |\mathbf{v}_\odot|$ and

$$\begin{aligned} h_0(l,b) = \frac{e^{-x_0^2}}{4\pi^{3/2}x_0 N_{\rm esc}} \Big\{ & 2(1+y_0^2) \\ & -\sqrt{\pi}e^{y_0^2} y_0(3+2y_0^2)[{\rm erf}(\sqrt{z_0^2+y_0^2-x_0^2}) - {\rm erf}(y_0)] \\ & -2e^{x_0^2-z_0^2}(1+4y_0^2+z_0^2-x_0^2-3y_0\sqrt{z_0^2+y_0^2-x_0^2})\Big\}. \end{aligned} \tag{9}$$

with $x_0 = v_\odot/\overline{v}_0$, $y_0 = -\mathbf{v}_\odot \cdot \hat{\mathbf{n}}/\overline{v}_0$, and $z_0 = v_{\rm esc}/\overline{v}_0$.

In the late-infall halo model SLI, the WIMPs belonging to stream i have all the same velocity $\mathbf{v}_i$ and they contribute a density ρ_i to the local WIMP density. The values of $\mathbf{v}_i$ and ρ_i are given in Table 1. The model of Ref. [6] does not include a velocity dispersion of the dark matter particles in the flows. In this case, the WIMP velocity distribution in the SLI model is

$$f_{\rm SLI}(\mathbf{v}) = \frac{1}{\rho} \sum_i \rho_i \, \delta(\mathbf{v} - \mathbf{v}_i). \tag{10}$$

The corresponding angular distribution of the WIMP flux simply consists of isolated points,

$$\frac{d\Phi_{\rm SLI}}{d\Omega} = \sum_i \frac{\rho_i u_i}{m} \, \delta(\hat{\mathbf{u}}_i + \hat{\mathbf{n}}). \tag{11}$$

Here $\mathbf{u}_i = \mathbf{v}_i - \mathbf{v}_\odot$, $u_i = |\mathbf{u}_i|$, and $\hat{\mathbf{u}}_i = \mathbf{u}_i/u_i$. If we introduce by hand a velocity dispersion $\overline{v}_i/\sqrt{2}$ for each flow, and assume a gaussian distribution of velocities for each flow, the velocity distribution becomes

$$f_{\overline{\rm SLI}}(\mathbf{v}) = \sum_i \frac{\rho_i}{\rho \pi^{3/2} \overline{v}_i^3} \, e^{-\mathbf{v}^2/\overline{v}_i^2}, \tag{12}$$

and the WIMP flux per unit solid angle

$$\frac{d\Phi_{\overline{\rm SLI}}}{d\Omega} = \sum_i \frac{\rho_i u_i}{m} \, h_i(l,b), \tag{13}$$

where

$$h_i(l,b) = \frac{e^{-x_i^2}}{4\pi^{3/2} x_i} \Big\{ 2(1+y_i^2) - \sqrt{\pi} e^{y_i^2} y_i (3+2y_i^2)[1 - {\rm erf}(y_i)] \Big\} \tag{14}$$

with $x_i = u_i/\overline{v}_i$ and $y_i = \mathbf{u}_i \cdot \hat{\mathbf{n}}/\overline{v}_i$. In the examples below, we set $\overline{v}_i = 30$ km/s.

Figs. 1 and 2 show sky maps of the flux of dark matter particles in the standard halo model (Fig. 1) and in the SLI halo model (Fig. 2). These are the fluxes according to an observer at rest with the solar system. The sky maps in Figs. 1 and 2 are equal-area projections of the celestial sphere in galactic coordinates.[1] The galactic center is at the center, the galactic north (south) pole is at the top (bottom), the galactic plane is horizontal passing through the center of the map. The Sun is moving towards the direction indicated by the white cross (Sun apex). The white circle indicates the direction opposite to the Sun's motion (Sun anti-apex). The color in the maps shows the intensity of the WIMP flux coming from each direction (a lighter color indicates a larger intensity).

[1] They are Mollweide projections. The relationship between the coordinates (x,y) on the map and the galactic coordinates (b,l) is $x = -(2\sqrt{2} l \cos\theta)/\pi$, $y = \sqrt{2}\sin\theta$, where θ is given by $2\theta + \sin(2\theta) = \pi \sin b$. The inverse formulas are $b = \arcsin\{[(2\theta + \sin(2\theta)]/\pi\}$, $l = -(\pi x)/(2\sqrt{2}\cos\theta)$, where $\theta = \arcsin(y/\sqrt{2})$.

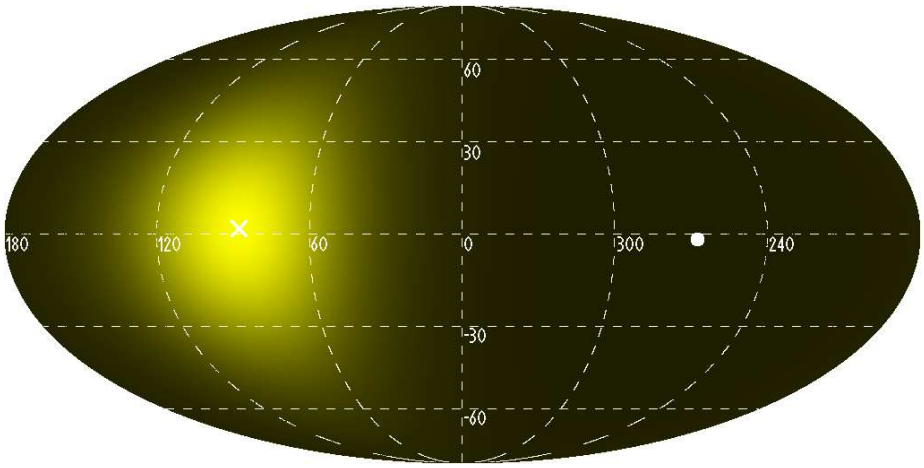

Figure 1: Sky map in galactic coordinates of the WIMP flux as seen by an observer moving with the Sun for the standard halo model with $\overline{v} = 220$ km/s and $v_{\rm esc} = 650$ km/s. Lighter colors indicate larger flux intensities. The WIMP wind comes mostly from the direction of the Sun motion (white cross).

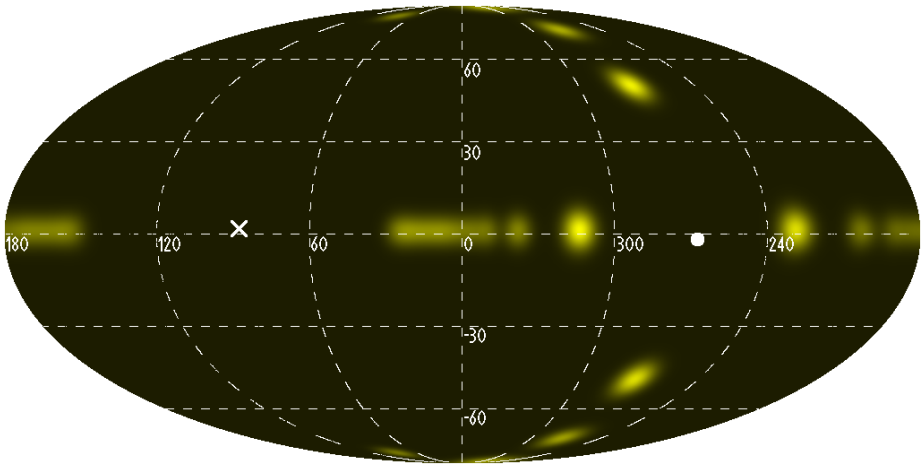

Figure 2: Sky map in galactic coordinates of the WIMP flux as seen by an observer moving with the Sun for Sikivie's late-infall halo model, smoothing each stream with a gaussian with velocity dispersion $\overline{v}_i = 30$ km/s. Lighter colors indicate larger flux intensities. WIMPs come from the direction of the streams (the bright spots). The most intense streams lie around the direction opposite to the Sun motion (white circle). This reverses the phase of the annual modulation of a halo WIMP signal due to the motion of the Earth around the Sun.

In the standard halo model of Fig. 1, most WIMPs come from the direction towards which the Sun is moving. In the SLI model of Fig. 2, WIMPs come from the direction of the streams (the bright spots). In the figure, each stream has been convolved with a Maxwellian velocity distribution with velocity dispersion $\overline{v}_i = 30$ km/s (otherwise the WIMPs of each stream would come only from one point in the sky). Fig. 2 clearly shows that in the SLI halo model most WIMPs come from directions in the hemisphere opposite to the Sun motion. As a consequence, the average "WIMP wind" velocity on Earth, as pointed out by Sikivie himself in Ref. [6], is reversed with respect to that in the standard halo model. This is because most halo particles in the SLI model move in the direction of the Sun's motion with a speed larger than that of the Sun. Therefore in the SLI model the annual modulation of a galactic WIMP signal has a phase opposite to the one usually assumed. Notice in Fig. 2 that in the SLI halo model many WIMPs come to Earth also from directions above and below the galactic plane. The directions of the streams form a characteristic "diamond" or "quad" pattern around the Sun anti-apex: the most intense WIMP fluxes are concentrated on the galactic plane and on the $l = 270^\circ$ meridian.

3 Annual Modulation of WIMP Fluxes

The time dependence of the galactic WIMP signal arises from the annual variation of the Earth velocity with respect to the Sun. Direct detection experiments lacking directional capabilities are sensitive to the WIMP flux integrated over the whole sky. This sky-integrated flux is the product of the local WIMP number density and of the mean speed of the WIMPs with respect to the Earth. It's the latter that is modulated. So here we study the time variations of the mean WIMP speed with respect to the Earth. (Notice that this is the mean speed, not the mean velocity.)

First we write an expression for the velocity of the Earth. We neglect the ellipticity of the Earth orbit and the non-uniform motion of the Sun in right ascension (an error of less than 2 days in the position of the modulation maximum and minimum). Hence we write the velocity of the Earth in terms of the Sun ecliptic longitude $\lambda(t)$ as

$$\mathbf{v}_\oplus(t) = v_\oplus \left[\hat{\mathbf{e}}_1 \sin\lambda(t) - \hat{\mathbf{e}}_2 \cos\lambda(t)\right], \tag{15}$$

where $v_\oplus = 2\pi$A.U./yr $= 29.8$ km/s is the orbital speed of the Earth, and the unit vectors $\hat{\mathbf{e}}_1$ and $\hat{\mathbf{e}}_2$ are in the direction of the Sun at the spring equinox and at the summer solstice, respectively. In galactic coordinates,

$$\hat{\mathbf{e}}_1 = (-0.0670, 0.4927, -0.8676), \tag{16}$$

$$\hat{\mathbf{e}}_2 = (-0.9931, -0.1170, 0.01032). \tag{17}$$

The Sun ecliptic longitude $\lambda(t)$ can be expressed as a function of time t in years with $t = 0$ at January 1 as

$$\lambda(t) = 360^\circ\,(t - 0.218). \tag{18}$$

Here 0.218 is the fraction of year before the spring equinox (March 21).

We give now the mean WIMP speed with respect to the Earth. It is

$$\langle v(t)\rangle = \int u\, f_\oplus(\mathbf{u},t)\, d^3u, \tag{19}$$

where $f_\oplus(\mathbf{u},t)$ is the WIMP velocity distribution in the rest frame of the Earth. In terms of the velocity distribution in the galactic rest frame $f(\mathbf{v})$,

$$f_\oplus(\mathbf{u},t) = f(\mathbf{u}+\mathbf{v}_\odot+\mathbf{v}_\oplus(t)). \tag{20}$$

So we can also write

$$\langle v(t)\rangle = \int \left|\mathbf{v}-\mathbf{v}_\odot-\mathbf{v}_\oplus(t)\right| f(\mathbf{v})\, d^3v. \tag{21}$$

In the standard halo model, the mean WIMP speed on Earth results

$$\langle v_{\rm std}(t)\rangle = v_0(t)\, g_0(t), \tag{22}$$

where $v_0(t) = \left|\mathbf{v}_\odot+\mathbf{v}_\oplus(t)\right|$ and

$$g_0(t) = \frac{1}{N_{\rm esc}}\left[\frac{e^{-x_0^2}}{x_0\sqrt{\pi}} + \left(1+\frac{1}{2x_0^2}\right)\mathrm{erf}(x_0) - \sqrt{\frac{2}{\pi}}\frac{1+z_0^2+x_0^2/3}{x_0}e^{-z_0^2}\right] \tag{23}$$

with $x_0 = v_0(t)/\overline{v}_0$ and $z_0 = v_{\rm esc}/\overline{v}_0$.

In the SLI halo model with no velocity dispersion,

$$\langle v_{\rm SLI}(t)\rangle = \sum_i \frac{\rho_i v_i(t)}{\rho} \tag{24}$$

with $v_i(t) = |\mathbf{v}_i-\mathbf{v}_\odot-\mathbf{v}_\oplus(t)|$. Including a velocity dispersion as described above,

$$\langle v_{\overline{\rm SLI}}(t)\rangle = \sum_i \frac{\rho_i v_i(t)}{\rho}\, g_i(t), \tag{25}$$

where

$$g_i(t) = \frac{e^{-x_i^2}}{x_i\sqrt{\pi}} + \left(1+\frac{1}{2x_i^2}\right)\mathrm{erf}(x_i) \tag{26}$$

with $x_i = |\mathbf{v}_i-\mathbf{v}_\odot-\mathbf{v}_\oplus(t)|/\overline{v}_i$.

We have plotted the mean WIMP speed $\langle v(t)\rangle$ as a function of time in Fig. 3 for the standard halo model and the SLI halo model with and without a velocity dispersion. The time axis starts January 1 and covers a year.

Fig. 3 clearly shows that the modulation in Sikivie's late-infall halo model has a phase opposite to the modulation in the standard halo model. The maximum of the mean WIMP speed on Earth occurs in early June in the standard model but in early December in Sikivie's late-infall halo model. With our assumptions and approximations, the maximum mean speed occurs June 1 in the standard

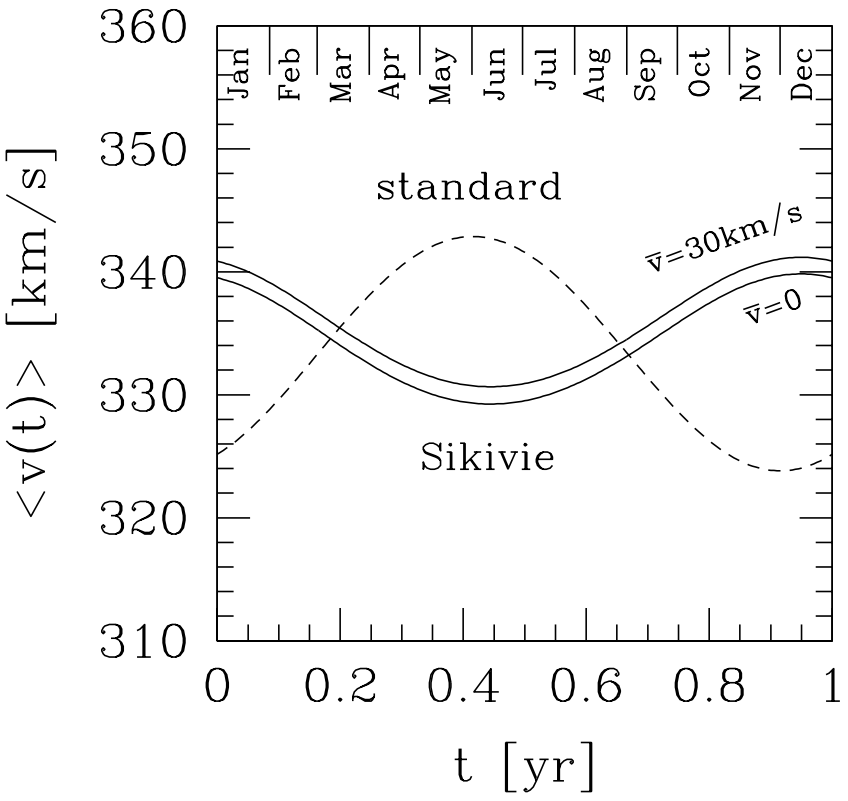

Figure 3: Annual modulation in the mean WIMP speed on Earth as a function of time. The time axis starts January 1 and covers a year. Solid curves in SLI halo model (we also include possible velocity dispersions); dashed curve in the standard halo model. The phase of the modulation is opposite in the two models.

model and December 12 in the SLI model; the minimum occurs December 1 in the standard model and June 11 in the SLI model. We remind the reader that the uncertainties in the Sun peculiar velocity and the approximations in the velocity of the Earth amount to an uncertainty of a few days in the position of the maxima and minima.

The change of phase in the modulation is independent of the velocity dispersion assumed in the SLI model. A dispersion of 30 km/sec gives very similar results to the zero dispersion (see Fig. 3). Even a dispersion of 220 km/s (not plotted), similar in magnitude to the average velocity, would give a phase of the modulation equal to the zero dispersion case (but the value of the average relative velocity would be much larger).

The local dark halo density in Sikivie's late-infall halo model, obtained by summing up the densities in each flow in Table 1, is ρ= 0.37 GeV/cm^3. The upper bounds on the scattering cross section for a particular WIMP depend on the value of the product $\rho\langle v(t)\rangle$. The bounds obtained with Sikivie's late-infall model and with a standard model with the same local density would differ by the ratio of WIMP velocities in Fig. 3. Otherwise the ratio of the local densities in both models should be taken into account.

4 Recoil-energy spectrum

The WIMP detection rate per unit detector mass and nucleus recoil energy in the range $(E, E + dE)$ can be written as

$$R(E) = \frac{\rho\sigma_0 F^2(q)}{m\mu^2}\eta(E,t). \tag{27}$$

Here σ_0 is a normalized WIMP-nucleus cross section; $\mu = mM/(m + M)$ is the reduced mass of the WIMP-nucleus system (m is the WIMP mass and M is the nucleus mass); $F(q)$ is a nuclear form factor function of the nucleus recoil momentum $q = 2ME$; $\eta(E,t)$ determines the annual modulation and depends only on the WIMP velocity distribution in the rest frame of the Earth $f_\oplus(\mathbf{u},t)$,

$$\eta(E,t) = \frac{1}{2}\int d\Omega_u \int_{\sqrt{ME/2\mu^2}}^{\infty} u\, f_\oplus(\mathbf{u},t)\, du. \tag{28}$$

The nuclear form factor $F(q)$ depends on the type of WIMP-nucleus interactions, namely if they are spin-dependent or spin-independent, and reflects the mass and spin distributions inside the nucleus. It may strongly affect the counting rates in dark matter detectors, but since it is time-independent it is inessential in the analysis of the annual modulation. Therefore in the examples below we set $F(q) = 1$. The recoil-energy spectra we plot should be multiplied by the appropriate $F(q)$.

We now focus on $\eta(E,t)$ since it is the only time dependent part in the recoil-energy spectrum due to WIMP-nucleus collisions. For the standard halo

model,

$$\eta_{\rm std}(E,t) = \frac{1}{N_{\rm esc}}\left\{\frac{1}{4v_\oplus(t)}\left[{\rm erf}\left(\frac{w+v_\oplus(t)}{\overline{v}_0}\right)-{\rm erf}\left(\frac{w-v_\oplus(t)}{\overline{v}_0}\right)\right] - \frac{1}{\pi^{1/2}\overline{v}_0}e^{-v_{\rm esc}^2/\overline{v}_0^2}\right\} \quad (29)$$

with $w=\sqrt{ME/2\mu^2}$. In Sikivie's late-infall model without velocity dispersion, each flow contributes a flat spectrum up to the maximum recoil energy

$$E_{{\rm max},i}(t) = \frac{2\mu^2}{M}\left|\mathbf{v}_i-\mathbf{v}_\odot-\mathbf{v}_\oplus(t)\right|^2. \quad (30)$$

The resulting spectrum is a series of steps where each step corresponds to a flow,

$$\eta_{\rm SLI}(E,t) = \sum_i \frac{\rho_i}{\rho}\,\frac{\theta(E_{{\rm max},i}(t)-E)}{2|\mathbf{v}_i-\mathbf{v}_\odot-\mathbf{v}_\oplus(t)|}. \quad (31)$$

Here θ is the Heaviside function. Notice that the position of the steps given by $E_{{\rm max},i}(t)$ depends on time, and so the end-point of each step is annually modulated.

In Fig. 4 we plot the recoil-energy spectra at the maximum and minimum of the modulation in the mean WIMP speed on Earth. At the lowest recoil-energies the phase of the modulation is opposite in the two models; at intermediate energies it is the same; at higher energies it is opposite again. To produce the figure we have assumed a local halo density $\rho = 0.3{\rm GeV}/c^2/{\rm cm}^3$, a WIMP mass $m = 60{\rm GeV}/c^2$, a ^{73}Ge detector, a WIMP-nucleus cross section $\sigma_0 = 10^{-35}{\rm cm}^2$, and a nuclear form factor $F(q) = 1$. Corresponding spectra for other detectors can be obtained using the relations $E' = (\mu'/\mu)^2(M/M')E$ and $R' = F^2(q)(\sigma_0'/\sigma_0)(\mu/\mu')^2R$.

One may worry that the lowest-energy step does not persist when additional flows with smaller velocities are added in the SLI model. We argue that this will not happen because while their velocities are smaller and smaller in the galactic rest frame they are not smaller and smaller in the Sun or Earth rest frames (see column 5 of Table 1). Hence the end-point of the lowest-energy step, which corresponds to the flow with the smallest speed relative to the Earth, will not change if additional flows above the 20th are added in the model.

Fig. 5 shows how the recoil-spectrum is modulated at fixed recoil-energies $E = 15, 25, 35$ keV. The change of phase of the modulation is again visible. It is also clear that except at the lowest recoil energies the spectral modulation in the SLI halo model is no longer well approximated by a sinusoidal function. This is due to the modulation of the position of the steps at $E_{{\rm max},i}(t)$ mentioned above. If particle flows are introduced in the halo model, a more general analysis of the experimental data than that used up to now may be called for.

The effect of a velocity dispersion in each flow is to blur the end-point of each step. The recoil-spectrum in the SLI model with velocity dispersion can

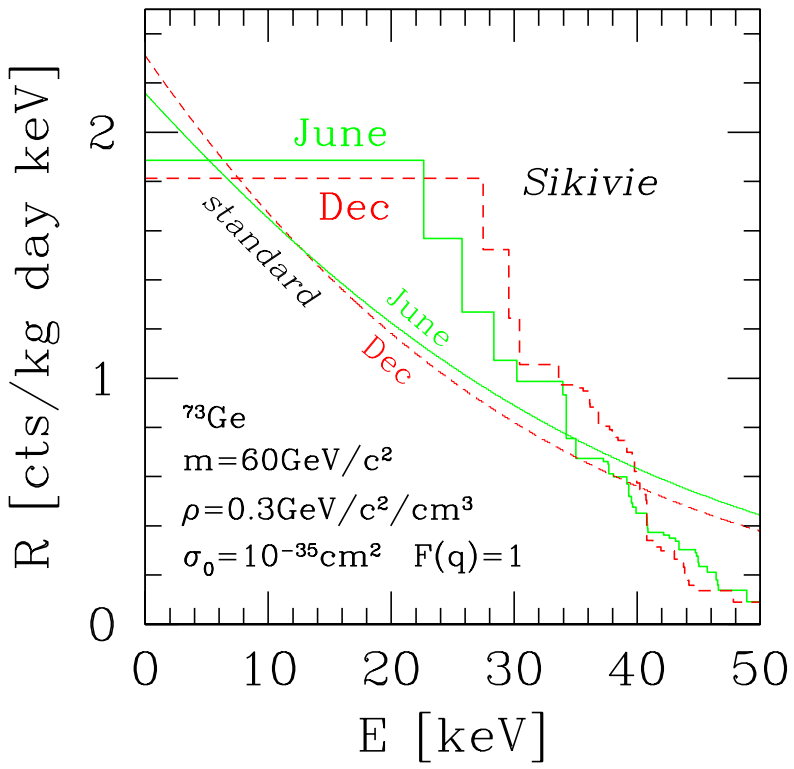

Figure 4: Recoil-energy spectrum at the maximum and minimum of the annual modulation in the mean WIMP speed on Earth. Step-like curves in the Sikivie's late-infall halo model; smooth curves in the standard halo model. The phase of the modulation in the two models is opposite at low energies, the same at intermediate energies, opposite again at high energies. Notice that the end-point energy of each step in the SLI model is annually modulated.

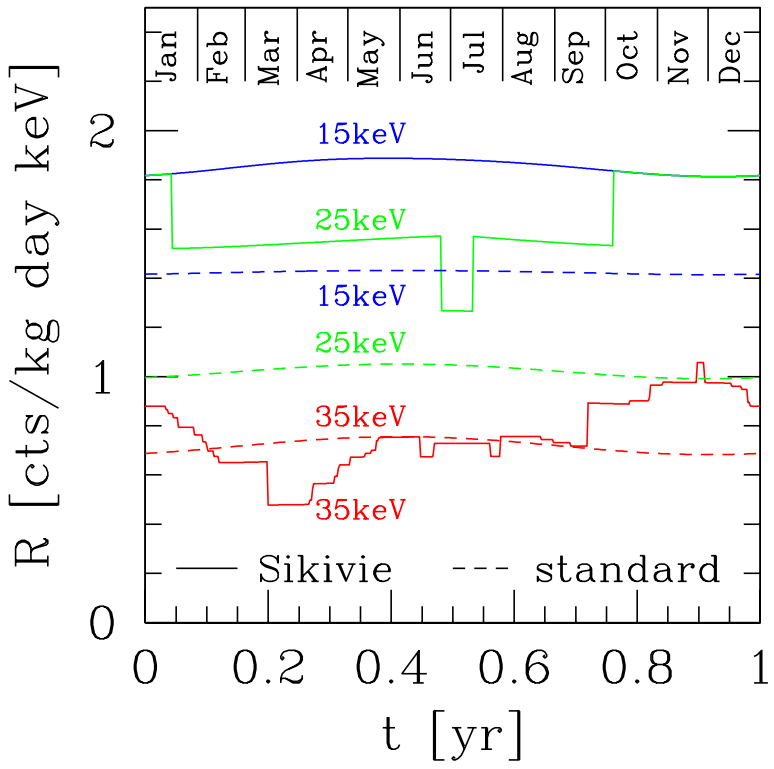

Figure 5: Annual modulation of the recoil-energy spectrum at several fixed energies. Solid curves in the Sikivie's late-infall halo model; dashed curves in the standard halo model. Beyond the end-point energy of the lowest step, the modulation of the recoil-energy spectrum in the SLI halo model may be poorly approximated by a sinusoidal (cfr. the 25keV curve, e.g.).

be obtained using the expression of $\eta_{\rm std}(E,t)$ after taking the limit $v_{\rm esc} \to \infty$ and replacing $1/N_{\rm esc} \to \sum_i \rho_i/\rho$ and $v_\oplus(t) \to |\mathbf{v}_i - \mathbf{v}_\odot - \mathbf{v}_\oplus(t)|$.

In Sikivie's model there is no virialized halo component. If one should exist, as assumed in Ref. [7], the local halo velocity distribution and local WIMP fluxes would be a combination of both components. This would result in a superposition with some relative amplitude of the fluxes and rates shown in Figs. 1, 2, 4, and 5. The phase of the annual modulation would then depend on the relative strength of both components.

5 Conclusions

The late-infall model [3] of halo formation, modified in recent years by P. Sikivie and collaborators [4, 5, 6] to include a net angular momentum and axial symmetry around its direction, predict non-virialized flows of dark matter particles falling into the galaxy and oscillating in and out many times. Hence it predicts a local velocity distribution completely different from the standard truncated Gaussian usually assumed. P. Sikivie in Ref. [6] has given the local velocities and densities of the first twenty pairs of flows (the first pair corresponding to particles coming for the first time into the galaxy from opposite sides of it, the second to those passing for the second time, etc.) in his particular late-infall model that has parameters that fit well the halo of our galaxy. In this model most WIMPs come from directions in the hemisphere opposite to the Sun motion. Namely the average "WIMP wind" velocity on Earth (as pointed out by Sikivie himself [6]) is reversed with respect to that in the standard halo model. Thus, in Sikivie's halo model, the annual modulation of a galactic WIMP signal has a phase opposite to the usually assumed. This was illustrated in Fig. 3. Moreover (as shown in Fig. 2) many WIMPs in this halo model approach the Sun and the Earth from directions above and below the galactic plane, with a clear pattern of directions. This would be very important for experiments in which directionality could be measured.

The main message we want to convey is that if a non-virialized halo component due to the infall of (collisionless) dark matter particles cannot be rejected, an annual modulation in a dark matter signal should be looked for by experimenters without fixing the phase a-priori. The detection of an annually modulated dark matter signal would not only reveal the nature of the dark matter in our halo, but the structure of the dark matter halo itself.

Acknowledgements

We thank the Aspen Center for Physics where this work was discussed with P. Sikivie last June. As we finished writing this paper, a similar work by A.M. Green appeared [8]: we basically agree with her conclusions where we overlap.

References

[1] A. Drukier, K. Freese and D. Spergel, Phys. Rev. D33, 3495 (1986).

[2] F. Mignard, A&A 354, 522 (2000); R.P. Olling and M.R. Merrifield, MNRAS 297, 943 (1998); M. Feast, F. Pont, and P. Whitelock, MNRAS 298, L43 (1998); A. Ali and M.A. Sharaf, New Astronomy 3, 419 (1998); W. Dehnen and J.J. Binney, MNRAS 298, 387 (1998); M. Feast and P. Whitelock, MNRAS 291, 683 (1997); D.W. Evans and M. Irwin, MNRAS 277, 820 (1995); F. Comerón, J. Torra, and A.E. Gómez, A&A 286, 789 (1994).

[3] J.E. Gunn and J. R. Gott, Ap. J. 176, 1 (1972); J. Fillmore and P. Goldreich, Ap. J. 281, 1 (1984); E. Bertschinger, Ap. J. 58, 39 (1985).

[4] J. Ipser and P. Sikivie, Phys. Lett. B 291, 288 (1992).

[5] P. Sikivie, I. Tkachev and Y. Wang, Phys. Rev. Lett. 75, 2911 (1995); Phys. Rev. D56, 1863 (1997); P.Sikivie, Phys. Rev. D60, 063501 (1999); W. Kinney and P. Sikivie Phys. Rev. D61, 087305 (2000).

[6] P. Sikivie, Nucl. Phys. Proc. Suppl. 72, 110 (1999).

[7] C.J. Copi, J. Heo, and L.M. Krauss, Phys. Lett. B461, 43 (1999); C.J. Copi and L.M. Krauss, astro-ph/0009467.

[8] A.M. Green, astro-ph/0012393.